Low-cost multimodal light sheet microscopy for optically cleared tissues and living specimens

Vincent Rouger
Ricardo Alchini
Alexei Kazarine
Angelica A. Gopal
Marie-Pier Girouard
Alyson E. Fournier
Paul W. Wiseman

SPIE.

Low-cost multimodal light sheet microscopy for optically cleared tissues and living specimens

Vincent Rouger,[a] Ricardo Alchini,[b] Alexei Kazarine,[a] Angelica A. Gopal,[a] Marie-Pier Girouard,[b]
Alyson E. Fournier,[b] and Paul W. Wiseman[a,c,*]
[a]McGill University, Department of Chemistry, 801 Sherbrooke Street, West, Montreal, Quebec H3A 0B8, Canada
[b]McGill University, Montreal Neurological Institute, Department of Neurology, 3801 University Street, Montreal, Quebec H3A 2B4, Canada
[c]McGill University, Department of Physics, 3600 University Street, Montreal, Quebec H3A 2T8, Canada

Abstract. Light sheet microscopy techniques have expanded with designs to address many new applications. Due to rapid advancements in computing power, camera/detector technologies, and tissue clearing techniques, light sheet methods are becoming increasingly popular for biomedical imaging applications at the cellular and tissue levels. Light sheet imaging modalities couple rapid imaging rates, low-levels of phototoxicity, and excellent signal to noise ratios, contributing to their popularity for experimental biology. However, the current major limitation of light sheet microscopy arises from optical aberrations, with the main drawback being the defocusing introduced by refractive index variations that accompany clearing techniques. Here, we propose an inexpensive and easy to build light sheet based instrumentation to overcome this limitation by optomechanically decoupling the sample scanning movement from the detection step. Our solution is relatively simple to implement and also provides increased modularity by using a swappable excitation arm. This expands the range of samples we can image on a single system, from high resolution for single cells at μm spatial resolution, to tissues with mm spatial resolution. We demonstrate our approach, using the system to image iDISCO cleared embryos and sciatic nerves, and provide the full three-dimensional reconstruction of these objects in minutes. © *The Authors.*
Published by SPIE under a Creative Commons Attribution 3.0 Unported License. Distribution or reproduction of this work in whole or in part requires full attribution of the original publication, including its DOI. [DOI: 10.1117/1.JBO.21.12.126008]

1 Introduction

In recent years, there has been a tremendous number of new developments in optical microscopy techniques targeted at imaging different biological systems at a range of spatial and temporal scales, with each technique having its own intrinsic advantages and limitations. We focus on new developments in light sheet microscopy, also known as single plane or selective plane illumination microscopy.[1,2]

Light sheet illumination was developed at the start of the 20th century,[3] and is having a resurgence in popularity after the characterization of fluorescent proteins[4] and their rapid incorporation as genetically encoded visualization tools for biomedical microscopy applications.[5] Light sheet microscopes were designed to illuminate specimens with a thin light sheet resulting in intrinsic optical sectioning for fluorescence microscopy.[6–9] Recent developments have significantly increased the resolution of this imaging method using multiple angle detection to achieve isotropic reconstruction of the specimen[10,11] or via the implementation of lattice light sheet,[12] the use of Bessel beams to appreciably reduce the thickness of the illuminated plane while keeping a large field of view, and a combination of Bessel beam excitation with two-photon illumination.[13]

Applications of light sheet microscopy are rapidly increasing, especially for imaging larger samples, such as zebrafish,[14,15] fly embryos,[9,16] *C. elegans*,[17,18] and mouse organs or embryos.[19–21]

Due to the orthogonal illumination inherent to this technique, photobleaching and phototoxicity are significantly reduced compared with traditional laser scanning confocal microscopy,[9,22] and single plane illumination permits the reduction of background fluorescence with camera acquisition of the entire imaging plane. This mode of detection significantly increases the image acquisition speed in comparison to point scanning systems, enabling three-dimensional (3-D) reconstructions of macroscopic samples and tissues in reasonable time periods and is especially suited for the imaging of live specimens.

Concurrently, sample clearing techniques have recently been developed to transform cumbersome opaque specimens into transparent samples for the optical imaging of highly scattering tissues, such as entire mouse brains or embryos. This property allows the observation of these biological specimens without relying on tissue sectioning and manual reconstruction, a process that can be time consuming and sometimes inaccurate. We utilize one of the simplest, cost effective, and rapid clearing techniques, iDISCO, which uses organic solvents to clear the tissues.[23] However, dibenzyl ether (DBE), the final solvent of the protocol in which the sample is imaged, has a high-refractive index ($\sim$1.56), rendering most light sheet microscopes inoperable due to the change in refractive index between the objective and specimen. Some commercial solutions exist with specialized immersion objectives for water-based clearing techniques,[24,25] but these objectives are relatively expensive and cannot be used for solvent clearing. These objectives, in addition to classic immersion objectives, cannot be used directly with such solvents without damaging the objective.

*Address all correspondence to: Paul W. Wiseman, E-mail: paul.wiseman@mcgill.ca
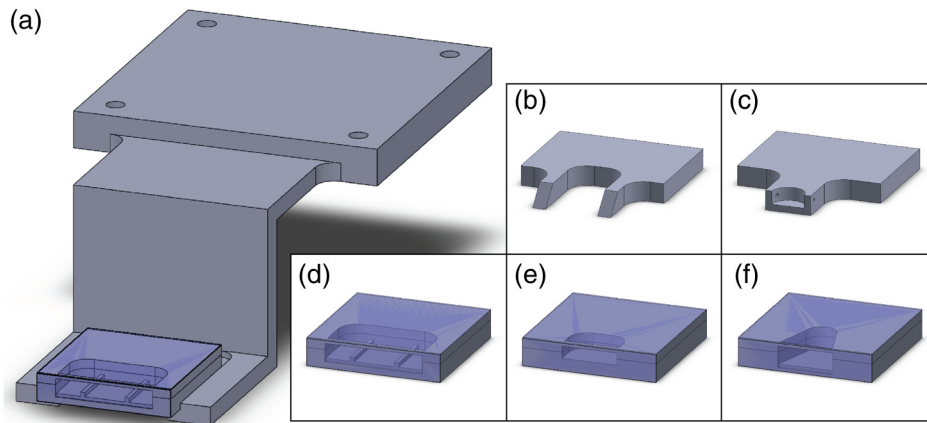
Fig. 1 3-D representation of sample holders with interchangeable ends developed for different sample types. (a) The sample holder arm has four holes on top to be fastened to the piezosystem, with an interchangeable sample holder on the front. (b) Sample holder for cells plated on coverslips. The middle of the holder is cut out to prevent laser reflections at the glass/acrylic interface. The coverslip is mounted at 45 deg to the sample holder to avoid perturbing the light sheet. (c) Sample holder for cells encapsulated in 3-D hydrogels, used to support a small cylinder of hydrogels. Holes on either side are needed to secure the hydrogels with a needle. (d) Sample holder for sciatic nerves, where the small protruding segments inside are needed to prevent the light sheet from being perturbed by the acrylic holder. (e) Sample holder for small organisms, e.g., zebrafish. (f) Sample holder for current mouse embryo experiments. All sample holder designs need to take into account the physical space required for the sample and the working distance of both objectives.

Here, we propose a new approach using a custom made holder which encases the sample and its medium in order to protect the objective (see Fig. 1). This overcomes limitations which would arise from direct contact solvent damage allowing us to mount standard objectives that can be used in conjunction with clearing solutions of any refractive index, in particular solvent-based clearing techniques. We implement our method using a simple modular passive light sheet design that incorporates an optomechanical decoupling of the excitation and detection objectives that enables us to image in organic solvents without a significant loss of resolution that would typically occur due to defocus from refractive index variations. We present the design and demonstrate applications of a system that is inexpensive, easy to build, and is scalable across sample type, size, and imaging medium.

2 Materials and Methods

2.1 Animals

SV129 mouse embryos imaged in this study were generously provided by Dr. Quenten Schwarz, University of Adelaide. Pregnant mice were euthanized at E11.5 and the embryos were collected, decapitated, and fixed in ice cold 4% paraformaldehyde (PFA) (Electron Microscopy Sciences, Hatfield, Pennsylvania) diluted in phosphate buffer saline (PBS) (141 mM NaCl, 2.7 mM KCl, 10 mM Na_2HPO_4, and 1.5 mM KH_2PO_4) overnight. For nerve preparations, adult C57BL/6 were raised according to the guidelines of the animal facility at the Montreal Neurological Institute. Adult mice were euthanized and nerves were collected and postfixed for 2 h in 4% PFA in PBS. Samples were washed in PBS and stored at 4°C prior to use.

2.2 Sample Preparation for Imaging

Whole mount fluorescent immunohistochemistry was performed according to a modified protocol.[23] Samples were dehydrated using a gradient of methanol (50%, 75%, 100%) diluted in PBS, incubating for 1 h per methanol solution. Autofluorescence was quenched by incubating samples overnight in an ice cold mixture of 70% methanol (Fischer Scientific, Geel, Belgium), 20% dimethylsulfoxide (DMSO) (Sigma, St. Louis, Missouri), and 10% hydrogen peroxide (Fisher Scientific, Fair Lawn, New Jersey).

Samples were rehydrated with methanol solutions in the reverse order (75%, 50%, and PBS) and fixed embryos were blocked at room temperature for 12 h in 6% donkey serum (Sigma, St. Louis, Missouri), and 0.1% Triton-100 (Sigma, St. Louis, Missouri) in PBS. For visualization of the spinal cord commissural projections, embryos were stained for Tag-1 (AF4439, R&D Systems, Minneapolis, Minnesota) 1:200 in wash solution (0.6% donkey serum, 0.1% Triton X-100 PBS) for 48 h at 37°C. Samples were vigorously washed for 12 h and subsequently incubated in Alexa 568 conjugated antigoat donkey (IgG A11056, Invitrogen, Eugene, Oregon) (1:250 in wash solution) for 36 h at 37°C. Finally, samples were washed for 12 h with PBS and kept at 4°C until imaging.

Nerve samples were prepared following a similar protocol. After methanol dehydration and peroxide bleaching, rehydrated samples were blocked at room temperature for 12 h in 10% goat serum (Sigma, St. Louis, Missouri) and 0.2% Triton-100 in PBS. Sciatic nerves were costained with mouse anti-βIII-Tubulin (801201, BioLegend, San Diego, California, 1:33 dilution) and rabbit SCG10 (Stathmin-2) (NBP149461, Novus Biologicals, Oakville, Canada, 1:200 dilution), in nerve wash solution (3% goat serum, 0.2% Triton-X, 10 μg/mL heparin in PBS) for 5 to 7 days at 37°C. After extensive washing, samples were incubated with Alexa 488 conjugated antimouse IgG (Invitrogen, Eugene, Oregon) and Alexa 568 conjugated anti-rabbit IgG, at a dilution of 1:33 and 1:200, respectively, for 5 to 7 days at 37°C. Finally, nerves were washed for 12 h in nerve wash solution and 30 min in PBS before storage at 4°C until clearing.

Clearing was performed in accordance with a previously described protocol.[26] Fluorescently stained embryos or nerves were first dehydrated using a tetrahydrofuran gradient (50%, 75%, and 100%) (Sigma, St. Louis, Missouri) at room temperature, for 1 h per solution. Samples were then immersed in DBE (Sigma, St. Louis, Missouri) for at least 30 min prior to imaging.

2.3 Cell Culture

Human embryonic kidney 293T cells were cultured in Dulbecco's modified Eagle's medium, supplemented with 10% fetal bovine serum, 4 mM L-glutamine, 100 units/mL penicillin, 0.1 mg/mL streptomycin, and 0.1 mM nonessential amino acids (Gibco, Carlsbad, California). Cells were maintained in a humidified 5% CO_2 atmosphere at 37°C. Cells were grown for 2 days on coverslips before imaging. At 24 h postplating, plasmids encoding transmembrane proteins attached to EGFP and mCherry were transfected into the cells using LTX Lipofectamine with the Plus Reagent, as specified by the manufacturer (Life Technologies, Carlsbad, California). Imaging was performed in media consisting of Hanks' balanced salt solution and 4-(2-hydroxyethyl)-1-piperazineethanesulfonic acid (Gibco, Carlsbad, California).

## 2.4 Interchangeable Sample Holder Design

Samples holders were designed (SOLIDWORKS, Waltham, Massachusetts) and cut out of acrylic sheets (1.5, 3, and 6 mm thick, Johnston Industrial Plastics, Montreal, QC, Canada) using a Roland MDX-40A CNC milling machine (Roland DGA Corporation, Irvine, California). Sample holders are displayed below in Fig. 1.

For encapsulation of samples containing DBE, two parts are milled, aligned, and assembled using acetone (ACP, Montreal, QC, Canada). After the sample holder has dried (∼10 min), a coverslip (#1) is attached to the front side using clear nail polish, and left to dry overnight. The attached coverslip is then shaped using a diamond burr to fit the front side of the holder.

2.5 Multimodal Light Sheet Setup with Dynamic Decoupling Between Excitation and Detection

We designed and built a highly modular system around a commercial microscope base creating a user-friendly light sheet microscopy system. We used a Nikon FN-1 upright microscope base (Nikon Canada Inc., Mississauga, ON, Canada), where the back left port of the NI-TT Quadrocular tilting tube on top of the microscope was used for detection. The microscope was equipped with halogen and mercury lamps for rapid sample visualization and positioning. An overview of the experimental setup for this microscope is shown below Fig. 2.

Imaging was performed with three different detection objectives for a variety of resolutions and fields of view; CFI Plan Apo Lambda 10× (0.45 NA, Nikon), CFI75 Apo LWD 25× (1.1 NA, Nikon), and CFO Apo 40× (0.8 NA, Nikon). A long travel objective piezoscanner (P-725.4CD, Physik Instrumente L.P., Auburn, Massachusetts) allowed rapid and reproducible movement of the objective lens. There are two main light pathways; 100% binocular and 100% camera port, with four different tube lenses (0.6×, 1×, 1.5×, 2×). The whole setup was assembled on an optical breadboard table (Newport Corporation, Irvine, California).
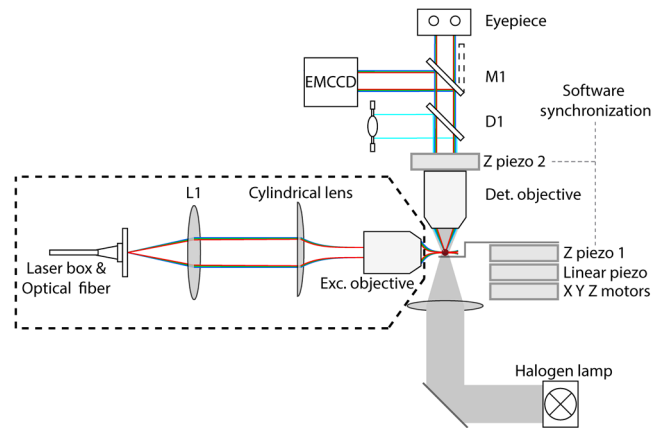

Fig. 2 Overview of the experimental setup. Layout showing the illumination path for brightfield (gray), fluorescence excitation and emission (dark blue, green, and red), and mercury lamp (cyan). Detection path is made of an objective, a Z piezoscanner, dichroic (D1), flipping mirror (M1), and an EM-CCD camera to record the filtered fluorescence signal coming from the sample. The gray dotted line represents the software synchronization between the sample and the detection objective. Light sheet generation is achieved using an optical fiber, lens (L1), cylindrical lens, and a 10× air objective or 40× immersion objective.

For excitation, we designed a laser box with five OBIS diode lasers (405, 445, 488, 561, 604 nm, Coherent Inc., Santa Clara, California) to cover excitation wavelengths for the majority of fluorophores, with two fibered and one free space outputs. All five laser lines were combined using reflective and dichroic mirrors, and directed to one of the three outputs using switchable mirrors. For light sheet use, the laser lines were focused onto a fiber (OZ Optics Ltd., Ottawa, ON, Canada) and the fiber output was directed to an excitation arm, where light was collimated using a lens and then shaped into a sheet of light via a cylindrical lens placed before a CFO Apo 40× (0.8 NA, Nikon) or CFI Plan Fluor 10× (0.3 NA, Nikon) excitation objective.[17] The excitation arms are assembled on a magnetic base to be easily interchangeable and are mounted on two linear stages to adjust the plane of light.

The sample holder module was placed on the right side of the microscope, opposite to the excitation arm, specially designed to fit the range of sample holders, Fig. 1, within the working distance of the appropriate objective. It was assembled on two sets of X, Y, and Z linear motors: one manual set for rapid sample positioning at the point of convergence between the excitation and detection objectives, and a second automated set for reproducible movement within the sample and sample stitching for larger fields of view. Additionally, two linear (X and Z) piezoactuators were added for fast 3-D imaging at nm step resolution. The system can also be modified for cuvette samples as shown in Fig. 3.

The entire setup, including excitation, detection, and all motorized parts, was controlled using LabVIEW and an NI-DAQ acquisition card (NI-PCIe-6353, National Instruments, Toronto, ON, Canada). The lasers, camera, and piezocontrollers are triggered using a digital or analog signal from the NI-DAQ for synchronization with the internal clock. Emitted photons are collected by the objective, filtered through a quad-band fluorescent cube (Chroma Technology Corp., Bellows Falls, Vermont), and detected on a 1024 × 1024 Andor iXon Ultra 888 EMCCD camera (SnowHouse Solutions Inc., Lac-Beauport, Quebec).
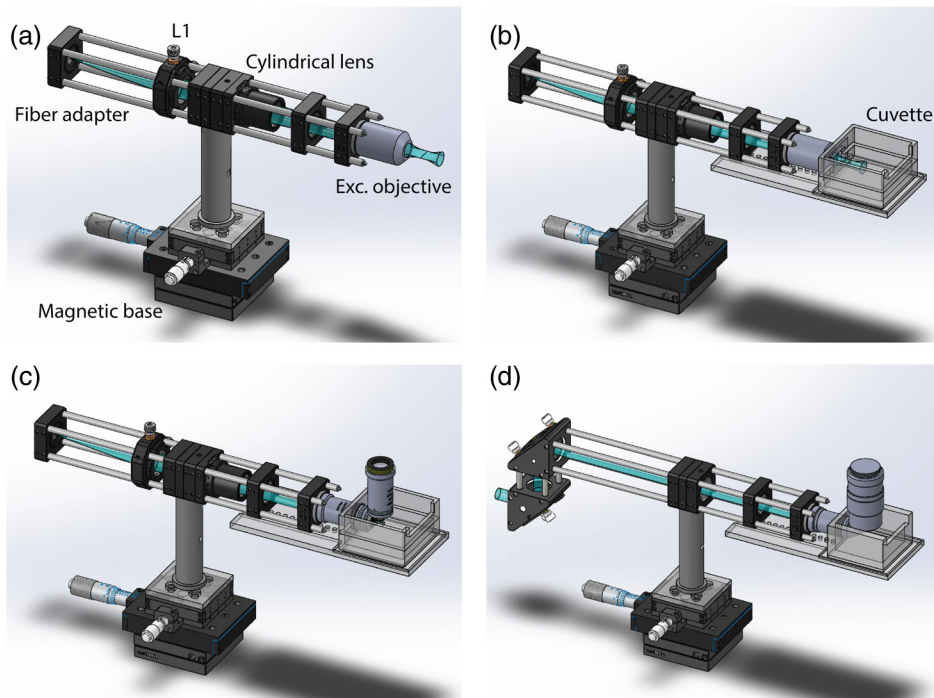
Fig. 3 Schematics of the different excitation arms developed for greater sample versatility. (a,b) Using the 10× excitation objective described before. The 10× objective can be used: (a) without or (b) with a cuvette with a cover slip on the side. (a) can be used with holders displayed in Figs. 1(d)–1(f), while (b) permits the use of Figs. 1(b) and 1(c) holders. No detection objective is shown on these two arms, because both can accommodate any detection objective due to a very long excitation working distance of 16 mm. (c) The 40× excitation arm in combination with the 40× detection objective. The cuvette was designed to hold a homemade PDMS O-ring in order to prevent leaks. A homemade support is used under the cuvette to prevent extra weight on the objective. In (a–c), the optical fiber is connected on the left side. (d) The excitation arm for the lattice light sheet using a custom objective for excitation[12] and the 25× detection objective. This arm serves to bring the laser excitation in at the correct height after passing through a complex optical path also described previously.[12]

A highly detailed supplementary file is available to any interested researcher via simple e-mail request. All parts are listed in this document with all CAD drawings and procedures for alignment and programming.

3 Results and Discussion

### 3.1 Combining Multiple Light Sheet Modes into One System

An important goal in microscope development is to design a way to combine many different modalities into one system. In the specific case of light sheet microscopy, the objective working distance is a limitation, as it needs to accommodate the sample size while maintaining a large numerical aperture for detection purposes. In the generation of a light sheet, only a section of the sheet can be considered homogenous, restricting the field of view. Furthermore, better resolution in the Z direction can only be achieved by decreasing the field of view, e.g., a light sheet thickness of 4 μm typically has a field of view of 300 μm, whereas to attain a thinner 1 μm sheet, the field of view will be reduced to 25 μm. To our knowledge, outside of high-end solutions such as isotropic multiview[10,11] or lattice light sheet[12] that can allow, respectively, a greater Z or both better Z and field of view, there is no solution to this trade-off. However, we introduce a very low cost simple adaptive solution which can be used on any sample size and desired resolution.

In our system, three different excitation arms are made easily interchangeable to fit the user's needs, see Fig. 3. The first excitation arm employs the 10× objective, Figs. 3(a) and 3(b), to provide a relatively large 300 μm field of view and a sizeable working distance of 16 mm, which can be used with any detection objective. The system can be easily adapted for imaging in a cuvette with a coverslip for side illumination, or for the homemade sample holders, shown in Fig. 1, to envelope specimens and protect objectives when used with organic solvents. However, this size excitation objective generates a sheet of ~4 μm.

The second excitation arm utilizes a 40× objective [Fig. 3(c)] with a working distance of 3.5 mm, which can only be used with an identical 40× detection objective. A cuvette is needed for the immersion of both objectives and a sample holder can be used to encase cleared samples in organic solvent, while protecting both objectives. The light sheet produced from this objective is ~1 μm thick, with a relatively small field of view of 25 μm.

3.2 Decoupling Excitation and Detection Planes

Here, we present a straightforward solution to compensate for changes in refractive index that can be easily implemented on the majority of light sheet systems. Clearing techniques are required for the imaging of relatively large samples with fluorescence microscopy. However, these methods often employ solvents with optical indices significantly different from the immersion liquid, i.e., water. Our implementation aims to
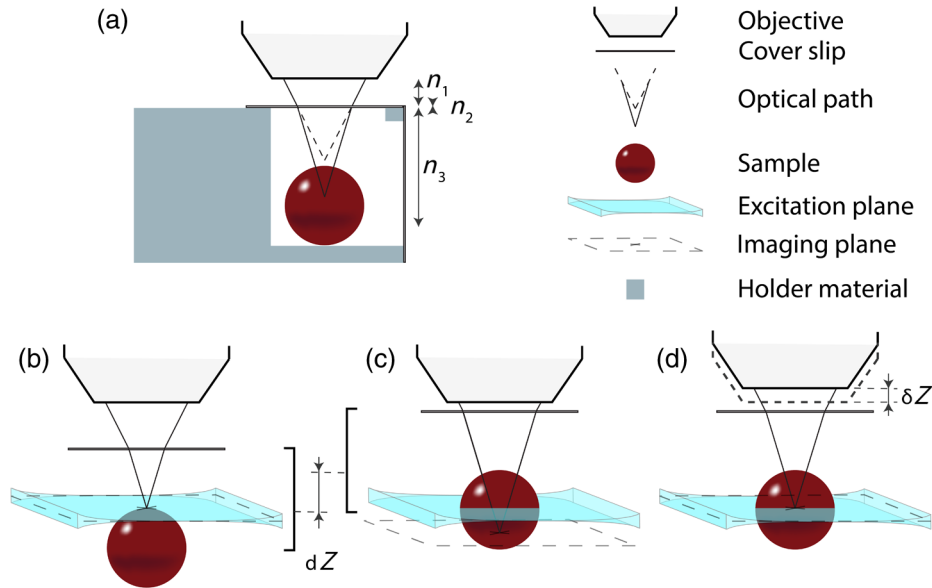
Fig. 4 Schematic of the optomechanical solution developed in order to image optically cleared samples in any solvent. (a) Schematic description of the sample holder used to protect objectives from the organic solvents. The specimen (red) is encapsulated in a custom designed holder (gray). Emitted light from the specimen passes through three media with different refractive indices before reaching the objective. The black line shows the light path if n_1 is air, n_2 is a borosilicate coverslip, and n_3 is DBE. The black dotted line illustrates the theoretical path if $n_1 = n_2 = n_3 = 1$. (b–d) The specimen and cover slip are moved together along the Z detection axis. dZ represents the displacement along this axis and δZ represents the correction for a given dZ movement using the piezoactuator. (b) The light sheet excitation plane (blue) is equivalent to the detection imaging plane (gray dotted lines) on the top of the specimen. (c) The specimen is moved up to acquire a different detection plane. Due to the change in refractive index, the excitation plane is no longer in the same position as the imaging plane, resulting in an unfocused image in Fig. 5(a). (d) To overcome this effect, we move the detection objective a calculated distance to recombine both planes.

overcome this limitation and can be applied to liquids of any refractive index.

When imaging in media with a different refractive index than that required for the detection objective, the detection cone [dotted line in Fig. 4(a)] is modified [solid line in Fig. 4(a)]. The numerical aperture and working distance for detection will be altered depending on the distance needed to travel through each medium to reach the objective. This can become problematic when scanning the sample along the detection axis. The defocusing effect of an index mismatch is illustrated in Figs. 4(b) and 4(c). As light sheet microscopy decouples excitation and detection into two objectives, when moving the sample the excitation and detection planes will quickly dissociate from each other. To compensate for the discrepancy in working distance, we implement a facile solution by relocating the objective Fig. 4(d), which recovers the overlap needed between the excitation sheet and detection plane.

3.3 Rapid Correction of the Imaging Plane

For correction of the imaging plane in fast acquisition mode (20 to 50 ms/frame), the objective needs to be rapidly repositioned for each frame. In our system, we implemented this via a piezoscanner for the objective to synchronize with the piezoactuator scanning the sample in the light sheet. Synchronization was made possible by simultaneously sending an analog signal via NI-DAQ to both piezosystems and a digital signal to the lasers and the camera.

For imaging in any refractive index medium, the compensation displacement of the objective is configured by the user determining the correct position for the piezoactuator for the top and the bottom of the Z stack in order to obtain a focused image.

When these parameters are known for a given imaging medium, the user can utilize the same displacement or redefine the parameters. During our experiments, a typical correction for the 10× objective in DBE is ∼85 μm for a 250 μm Z stack and ∼25 μm for the 40× objective. After user setup, the software simply divides the entire compensation displacement by N number of planes in the Z stack in order to apply the compensation during the imaging of each plane

$$\delta Z = \frac{(Z_{\text{top}} - Z_{\text{bottom}})}{N},$$

where δZ is the corrective displacement of the objective for a given dZ displacement of the sample and Z_{top} and Z_{bottom} represent the user defined top and bottom positions needed for the piezocorrection.

By using these live corrections, users can image in any refractive index environment and we have demonstrated this in DBE, Fig. 5. We show the detrimental impact on imaging without the piezoelectric correction, exhibited after a small displacement of 50 μm in Fig. 5(a), and we present the acquisition with the correction from our technique in Fig. 5(b), revealing structures that were previously obscured. Users can acquire large stacks without a loss of information or the need to
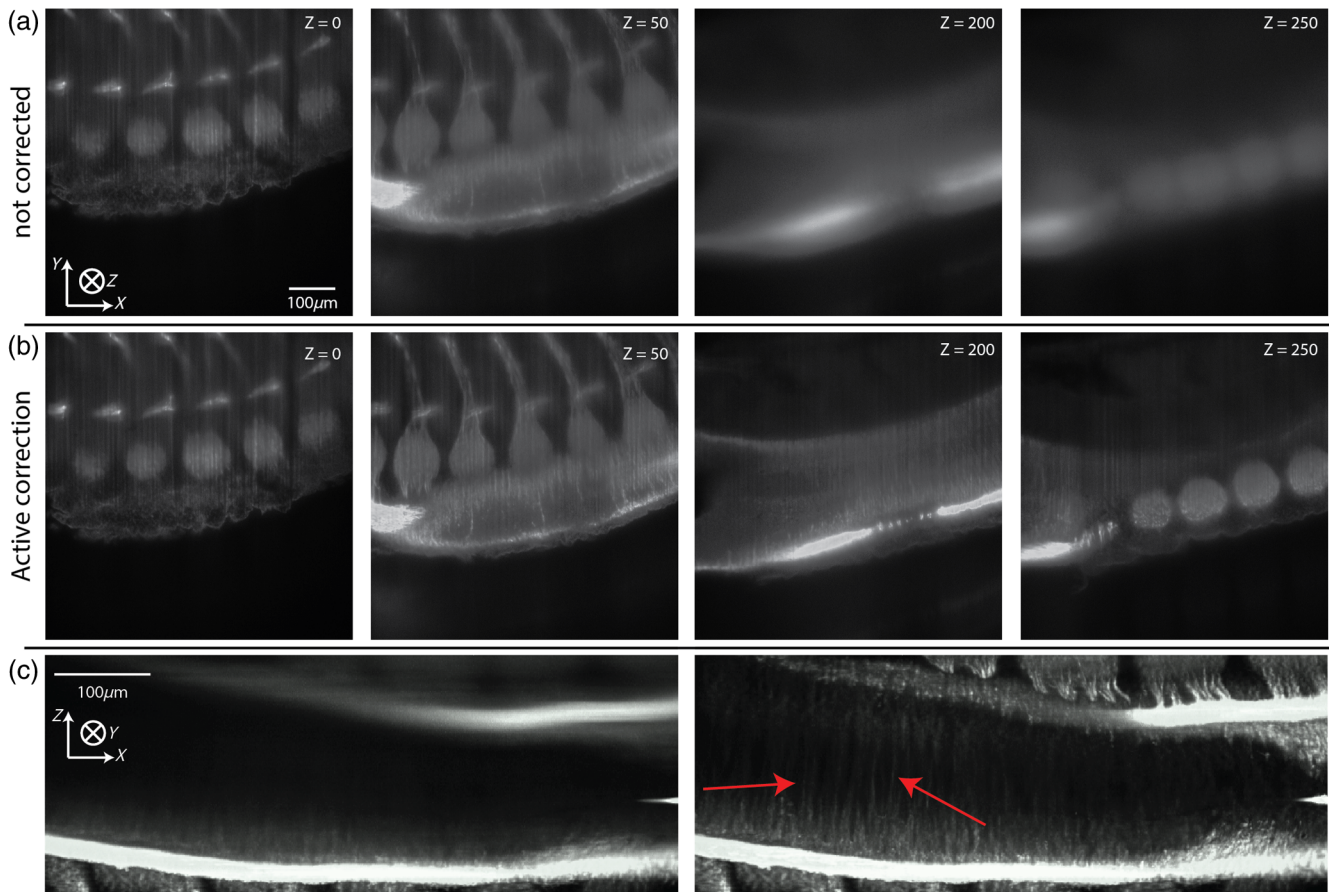
Fig. 5 Active refractive index correction on murine embryonic spinal cord and dorsal root ganglion neurons stained for Tag-1. (a,b) 250 μm Z stack acquisition on the same part of the same embryo (a) without and (b) with the plane-correction, which uses the displacement of the objective to correct for the high-refractive indices (DBE, $n = 1.56$). (c) A max projection was applied to highlight the axons. There is a noticeable difference in the fine commissural fibers as they can be observed from the inner part of the spinal cord without (left) and with (right) correction, obtained by reslicing the Z stack in (a/b) in the X and Y directions to view the back of the embryo. The correction allowed us to observe fine structures of these commissural tracts in detail (red arrows) and their parallel disposition in the ventral midline of the neural tube. X and Y resolution with this objective is limited by pixel size which is 650 nm. The Z resolution is limited by the light sheet axial dimension measured to be between 3.5 and 4 μm depending on the alignment and the Z stack is oversampled every 1 μm (Video 1, mp4, 5,689 KB) [URL: http://dx.doi.org/10.1117/1.JBO.21.12.126008.1].

periodically refocus. Video 1 highlights the same corrective implementation for 3-D imaging of a mouse embryo.

3.4 Acquisition of an Entire Specimen

When using the excitation arm equipped with the 10× objective, the field of view is considered to be ~300 μm (i.e., homogeneous part of the light sheet) by 650 μm (camera field of view) and the maximum movement of the piezoelectric actuator with respect to the Z stack is 250 μm. In order to record the entire specimen (i.e., 12.5-day mouse embryo, $4 \times 3 \times 3$ mm^3), the acquisition needs to take place over multiple fields of view. For this, we use three motorized stages to take Z stacks at different positions, crop each stack to keep the thinnest homogeneous part of the light sheet, and stitch the Z stacks together as shown in Fig. 6.

Automated data treatment for the acquisition of the entire specimen was performed using the Fiji stitching plugin[27] and 3-D rendered using Imaris (Bitplane, South Windsor, Connecticut). For the sample presented in Figs. 5 and 6, acquisition time was

around 10 min/mm^3. The acquisition time varies depending on the integration time and camera mode.

3.5 Neurobiology Applications

Spinal cord commissural neurons are an important model system for axon guidance in mammals. This population of neurons projects their axons radially toward the ventral midline, where they cross to the opposite hemicord and change their growth direction to the higher brain regions.[28] These directional changes make it difficult to quantify the different possible phenotypes for these axons. One limitation in the field is the need to physically slice the samples and perform immunostaining for the neuronal populations of interest, but this has recently been overcome by the development of clearing techniques.[23,26,29,30]

As hundreds of thousands of commissural neurons project in parallel, only an imaging system capable of resolving very fine structures would allow us to study the neuronal projections. This can be achieved by reducing the light scattering of the sample through clearing using a range of different chemicals that act by
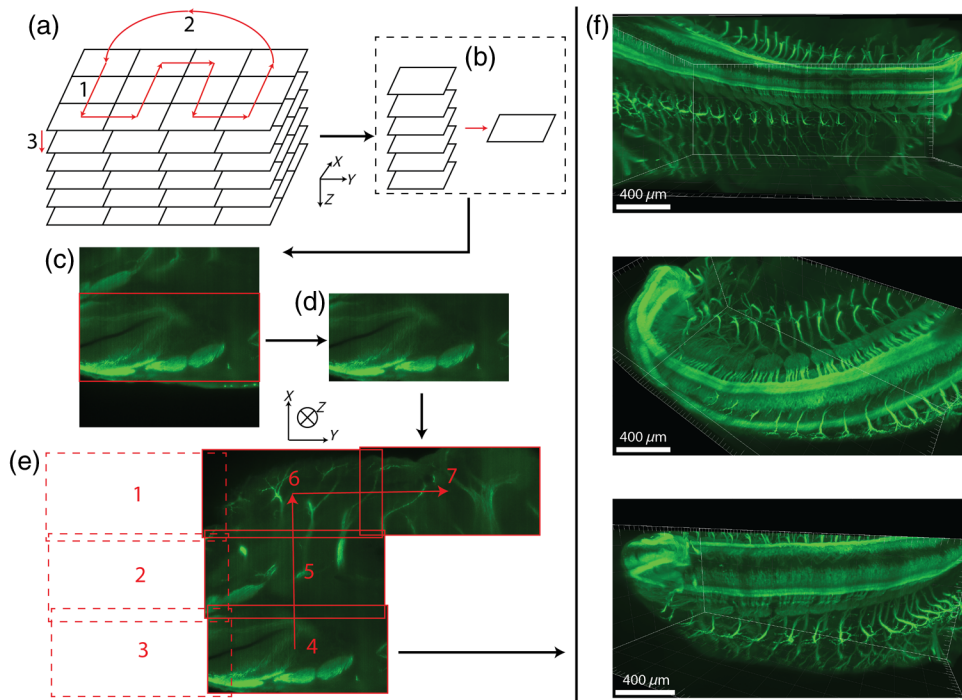
Fig. 6 Schematic for data treatment; process and stitching for a full 3-D rendering of a mouse embryo. Multiple full frame Z stacks of 250 μm are acquired following the order shown in (a) (where each square represents a 250 μm stack), in multiple X, Y, and Z positions. (b) For each X and Y position, the Z positions are concatenated into a single Z stack. (c) All Z stacks are cropped in X and Y, to only retain data collected from the thinnest part of the light sheet (d). (e) The cropped stacks are then stitched according to the motor displacements using Fiji stitching plugin.[27] (f) The entire specimen is rendered in Imaris. This 11.5-day mouse embryo sample was $1000 \times 2500 \times 1250 \times \mu m^3$. For dynamic view of the mouse embryo, see (Video 2, mp4, 14,198 KB) [URL: http://dx.doi.org/10.1117/1.JBO.21.12 .126008.2]. X and Y resolution with this objective is limited by pixel size which is 650 nm. The Z resolution is limited by the light sheet axial dimension measured to be between 3.5 and 4 μm depending on the alignment, and the Z stack is oversampled every 1 μm.

equilibrating refractive indices through the tissue.[31] Each clearing method uses a mounting medium with a specific refractive index[31] and this often poses a problem for microscope objectives, which are usually designed for a single refractive index.

As can be observed in Fig. 5(a), the structure of thick spinal cord commissural axons (~5 to 10 μm) is lost as we advance deeper in the DBE-immersed tissue. By mechanically correcting the focal plane deviation caused by DBE, we are able to visualize the crossing fibers in the midline, Fig. 5(c). To our knowledge, this is one of the sharpest images of the developing commissural spinal cord tracts. Using our method for focus correction, we were able to image all of the spinal cord commissural neurons using the general marker Tag-1, at a similar resolution to what has been previously published with neuronal subpopulation markers.[29] Thus, the imaging improvement brought by mechanical focal correction allows for a detailed inspection of spinal cord phenotypes without incurring a cell population bias in order to resolve the axons.

In addition, clearing techniques enable the observation of whole mouse embryos without tissue sectioning, Fig. 6. As the neurons in the spinal cord differentiate in waves, in which the cells at the brachial level mature earlier than the caudally located neurons,[32] it is advantageous to be able to resolve the complete structure. In comparison to commercially available light sheet microscopes, mechanical focal correction can be used to reach the same resolution without specific sample preparation constraints and index compatibility.

3.6 Nerve Imaging

The benefits of our correction method are readily apparent when applied to nerve imaging. Understanding how nerves develop and regenerate is a major challenge for the neuroscience field. The current gold standard method for this analysis is the manual sectioning of nerves in transverse or longitudinal sections and subsequent reconstruction. For a rodent nerve, that usually implies combining images of hundreds of slices from single nerves in order to find growing fibers. In such cases, one nerve can have a diameter of 0.5 mm and length of several centimeters. As the sectioning process transposes a 3-D system to two-dimensional fragments, it is susceptible to many interpretation mistakes, including the confusion of spared and regenerating fibers.[33]

While multiphoton and point scanning confocal microscopy have been used together with tissue clearing, these techniques are time consuming and can give rise to a significant bleaching problem.[34] These drawbacks can be overcome with spinning disk microscopy if pinhole crosstalk did not pose a challenge for scanning deep tissues.[35] To our knowledge, some of the best results for the imaging of regenerating nerves in whole mount preparations have been obtained by light sheet imaging of cleared tissue using organic solvents.[36,37] Here, we show that our system is capable of imaging both DBE- immersed sciatic nerves, which are important models for the study of the peripheral and central nervous systems, respectively. We can observe
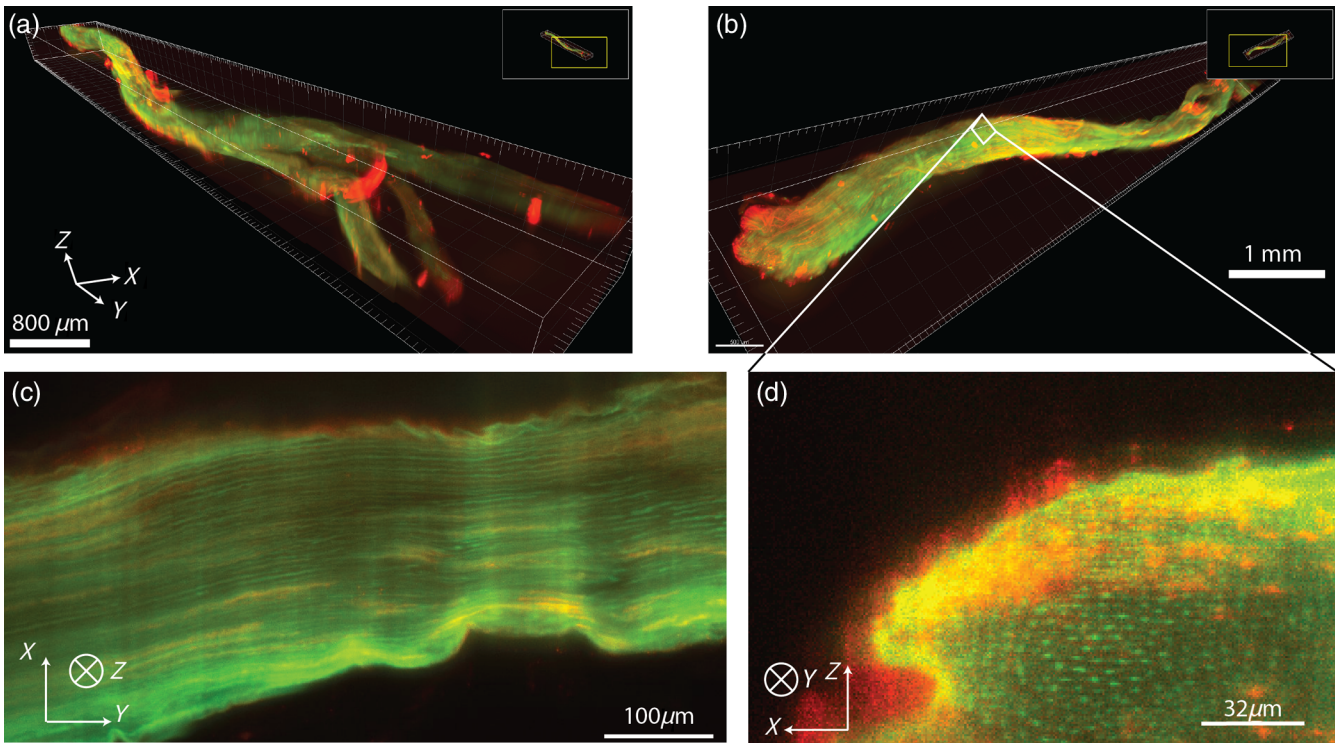
Fig. 7 (a,b) 3-D rendering of light sheet images representing the reconstruction on an intact mouse sciatic nerve, fluorescently tagged with Alexa 488 (β-III-Tubulin) and Alexa 584 (Stathmin 2). The entire sciatic nerve sample is $1050 \times 7900 \times 470$ μm^3. Total acquisition time in two color imaging was 1 h, including 36 positions for stitching. (c,d) The resolution of the light sheet enabled visualization of separate nerve fibers. (c) Max projection of several images of a stack showing optically separated nerve fibers. (d) Single image projection of a perpendicular nerve plane (Video 3, mp4, 14,197 KB) [URL: http://dx.doi.org/10.1117/1.JBO.21.12.126008.3] shows a 3-D reconstruction of the nerve. X and Y resolution with this objective is limited by pixel size which is 650 nm. The Z resolution is limited by the light sheet axial dimension measured to be between 3.5 and 4 μm depending on the alignment and the Z stack is over-sampled every 1 μm.

the expression of neuronal markers, such as β-III-tubulin, to follow axon morphology across an entire nerve, as shown in Fig. 7. Regenerating fibers can be identified by Stathmin-2 expression, a marker of growing and sensory axons,[38] also shown in Fig. 7. Our system could enable us to count and trace growing and regenerating fibers throughout the extension of the nerves.

Altogether, light sheet microscopy consists of a practical and accessible method to image whole mount preparations. Combined with paradigms of nerve lesion, this system can be used to accurately assess nerve regrowth in future studies.

3.7 Imaging of Live Single Cells

Equipping the light sheet microscope with 40× objectives for excitation and detection, alongside the 45 deg sample holder, Fig. 1(b), single cell imaging was achieved at a 3-D acquisition timescale of ms. However, using this objective, the field of view was limited to 20 to 30 μm. The piezoelectric actuators were completely synchronized, as one was used to scan the sample in the Z direction, while the other simultaneously moves the sample along the excitation axis in order to center the sample at the thinnest part of the light sheet for the best resolution. Images of single cells are shown in Fig. 8.

3.8 Implementation of Further Corrections

For compensation of the defocusing effect when stitching large specimens, the excitation arms can be further motorized along

the excitation axis, analogous to our solution employed to correct for excitation in high-refractive index media. In our system, the light sheet displacement along the excitation axis was almost negligible due to the numerical aperture and working distance of the objective used, therefore, we did not need to motorize this
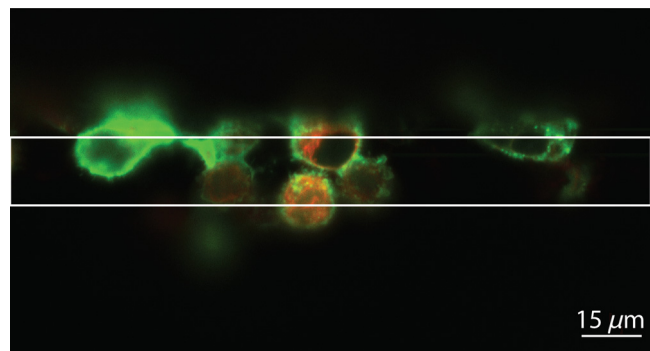
Fig. 8 Image of live HEK293T cells using the 40× objectives for both excitation and detection. The area between the white lines represents the area that is subjected to a homogenous light sheet (~25 μm). Crop of the camera field of view to show the effect of the light sheet edges. To acquire a Z stack, the X and Z piezosystems are used simultaneously to image on the 45 deg coverslip and for the thinnest part of the light sheet to be kept in the middle of the frame. To reconstruct the Z stack, the central part should be cropped and realigned, as the images are shifted by the X piezosteps.

part. However, other objectives would need this correction. The cropping of data to include only sampling from the thinnest part of the light sheet enables the best resolution possible.

Aberrations due to material scattering and absorption (i.e., stripes) can be avoided by the use of two light sheets, generated by two objectives on different sides of the sample,[8] by pivoting the cylindrical lens,[8] by implementing a rotational stage,[7,19,20] or by software treatment.[39] Currently, we are adding a third excitation arm, Fig. 3(d), to our modular system to enable the generation of a lattice light sheet, for improved resolution in Z while keeping a reasonable field of view.[12]

4 Conclusion

In conclusion, we have introduced and described a highly modular light sheet microscope design equipped with different excitation arms for a variety of imaging samples and conditions and a wide array of sample chambers/holders. Our goal is to enable interested readers to build their own light sheet systems, even with minimal knowledge of optics and programming, where the system is entirely flexible to image at different resolutions.

As described recently in a comprehensive review,[40] the best clearing techniques are challenging for microscopy due to the large indices of refraction for the solutions typically used. The system presented here enables users to work in any refractive index imaging medium by optomechanically decoupling the excitation and detection movement through a straightforward implementation of two synchronized piezoelectric actuators. Through our solution, we introduce live compensation along the detection axis during Z stack acquisition for every refractive index, enabling high resolution 3-D imaging of specimens cleared using a variety of techniques. To our knowledge, this is the first light sheet microscope to enable such versatility of imaging in media with varying refractive indices.

Disclosures

There are none.

References

1. P. A. Santi, "Light sheet fluorescence microscopy: a review," *J. Histochem. Cytochem.* **59**(2), 129–138 (2011).

2. M. Weber, M. Mickoleit, and J. Huisken, "Light sheet microscopy," *Methods Cell Biol.* **123**, 193–215 (2014).

3. H. S. A. R. Zsigmondy, "Über sichtbarmachung und grössenbestimmung ultramikroskopischer teilchen," *Ann. Phys.* **4**, 1–39 (1903).

4. O. Shimomura, F. H. Johnson, and Y. Saiga, "Extraction, purification and properties of aequorin, a bioluminescent protein from the luminous hydromedusan, Aequorea," *J. Cell Comp. Physiol.* **59**, 223–239 (1962).

5. R. Y. Tsien, "Nobel lecture: constructing and exploiting the fluorescent protein paintbox," *Integr. Biol.* **2**(2–3), 77–93 (2010).

6. J. A. Buytaert and J. J. Dirckx, "Design and quantitative resolution measurements of an optical virtual sectioning three-dimensional imaging technique for biomedical specimens, featuring two-micrometer slicing resolution," *J. Biomed. Opt.* **12**(1), 014039 (2007).

7. H. U. Dodt et al., "Ultramicroscopy: three-dimensional visualization of neuronal networks in the whole mouse brain," *Nat. Methods* **4**(4), 331–336 (2007).

8. J. Huisken and D. Y. Stainier, "Even fluorescence excitation by multi-directional selective plane illumination microscopy (mSPIM)," *Opt. Lett.* **32**(17), 2608–2610 (2007).

9. J. Huisken et al., "Optical sectioning deep inside live embryos by selective plane illumination microscopy," *Science* **305**(5686), 1007–1009 (2004).

10. R. K. Chhetri et al., "Whole-animal functional and developmental imaging with isotropic spatial resolution," *Nat. Methods* **12**(12), 1171–1178 (2015).

11. A. Kumar et al., "Dual-view plane illumination microscopy for rapid and spatially isotropic imaging," *Nat. Protoc.* **9**(11), 2555–2573 (2014).

12. B. C. Chen et al., "Lattice light-sheet microscopy: imaging molecules to embryos at high spatiotemporal resolution," *Science* **346**(6208), 1257998–1257998 (2014).

13. E. S. Welf et al., "Quantitative multiscale cell imaging in controlled 3D microenvironments," *Dev. Cell* **36**(4), 462–475 (2016).

14. P. J. Keller et al., "Reconstruction of zebrafish early embryonic development by scanned light sheet microscopy," *Science* **322**(5904), 1065–1069 (2008).

15. J. Swoger et al., "4D retrospective lineage tracing using SPIM for zebrafish organogenesis studies," *J. Biophotonics* **4**(1–2), 122–134 (2011).

16. R. Tomer et al., "Quantitative high-speed imaging of entire developing embryos with simultaneous multiview light-sheet microscopy," *Nat. Methods* **9**(7), 755–763 (2012).

17. C. Chardes et al., "Setting up a simple light sheet microscope for in toto imaging of C. elegans development," *J. Visualized Exp.* **87**, 51342 (2014).

18. Y. Wu et al., "Inverted selective plane illumination microscopy (iSPIM) enables coupled cell identity lineaging and neurodevelopmental imaging in Caenorhabditis elegans," *Proc. Natl. Acad. Sci. U. S. A.* **108**(43), 17708–17713 (2011).

19. V. Ermolayev et al., "Ultramicroscopy reveals axonal transport impairments in cortical motor neurons at prion disease," *Biophys. J.* **96**(8), 3390–3398 (2009).

20. N. Jahrling, K. Becker, and H. U. Dodt, "3D-reconstruction of blood vessels by ultramicroscopy," *Organogenesis* **5**(4), 227–230 (2009).

21. R. S. Udan et al., "Quantitative imaging of cell dynamics in mouse embryos using light-sheet microscopy," *Development* **141**(22), 4406–4414 (2014).

22. J. Huisken and D. Y. Stainier, "Selective plane illumination microscopy techniques in developmental biology," *Development* **136**(12), 1963–1975 (2009).

23. N. Renier et al., "iDISCO: a simple, rapid method to immunolabel large tissue samples for volume imaging," *Cell* **159**(4), 896–910 (2014).

24. V. Marx, "Microscopy: seeing through tissue," *Nat. Methods* **11**(12), 1209–1214 (2014).

25. A. Masson et al., "High-resolution in-depth imaging of optically cleared thick samples using an adaptive SPIM," *Sci. Rep.* **5**, 16898 (2015).

26. A. Erturk et al., "Three-dimensional imaging of solvent-cleared organs using 3DISCO," *Nat. Protoc.* **7**(11), 1983–1995 (2012).

27. S. Preibisch, S. Saalfeld, and P. Tomancak, "Globally optimal stitching of tiled 3D microscopic image acquisitions," *Bioinformatics* **25**(11), 1463–1465 (2009).

28. P. H. Dos Santos et al., "Effect of thermocycling on roughness of nanofill, microfill and microhybrid composites," *Acta Odontol. Scand.* **73**(3), 176–181 (2015).

29. M. Belle et al., "A simple method for 3D analysis of immunolabeled axonal tracts in a transparent nervous system," *Cell Rep.* **9**(4), 1191–1201 (2014).
30. K. Chung and K. Deisseroth, "CLARITY for mapping the nervous system," *Nat. Methods* **10**(6), 508–513 (2013).
31. D. S. Richardson and J. W. Lichtman, "Clarifying tissue clearing," *Cell* **162**(2), 246–257 (2015).
32. O. Kiehn and S. J. Butt, "Physiological, anatomical and genetic identification of CPG neurons in the developing mammalian spinal cord," *Prog. Neurobiol.* **70**(4), 347–361 (2003).
33. O. Steward, B. Zheng, and M. Tessier-Lavigne, "False resurrections: distinguishing regenerated from spared axons in the injured central nervous system," *J. Comp. Neurol.* **459**(1), 1–8 (2003).
34. P. Pantazis and W. Supatto, "Advances in whole-embryo imaging: a quantitative transition is underway," *Nat. Rev. Mol. Cell Biol.* **15**(5), 327–339 (2014).
35. T. Shimozawa et al., "Improving spinning disk confocal microscopy by preventing pinhole cross-talk for intravital imaging," *Proc. Natl. Acad. Sci. U. S. A.* **110**(9), 3399–3404 (2013).
36. A. Erturk et al., "Three-dimensional imaging of the unsectioned adult spinal cord to assess axon regeneration and glial responses after injury," *Nat. Med.* **18**(1), 166–171 (2012).
37. A. Erturk, D. Lafkas, and C. Chalouni, "Imaging cleared intact biological systems at a cellular level by 3DISCO," *J. Visualized Exp.* (89), (2014).
38. S. Chauvin and A. Sobel, "Neuronal stathmins: a family of phospho-proteins cooperating for neuronal development, plasticity and regeneration," *Prog. Neurobiol.* **126**, 1–18 (2015).
39. U. Leischner et al., "Formalin-induced fluorescence reveals cell shape and morphology in biological tissue samples," *PLoS One* **5**(4), e10391 (2010).
40. L. Silvestri et al., "Clearing of fixed tissue: a review from a microscopist's perspective," *J. Biomed. Opt.* **21**(8), 081205 (2016).

Vincent Rouger received his BSc degree in physics and chemistry from Burgundy University in 2005 and his PhD in immunology from Aix Marseille University at the Centre d'Immunologie de Marseille Luminy in 2013. Currently, he is working as a postdoctoral fellow in Professor Wiseman's laboratory in the Chemistry Department at McGill University.

Ricardo Alchini received his BSc degree in biological sciences from the Federal University of Santa Catarina in 2008 and his MSc degree in frontier biosciences from Osaka University in 2011. Currently, he is a PhD candidate in Professor Fournier's laboratory in the Montreal Neurological Institute at McGill University.

Alexei Kazarine received his BSc (Hons) degree in chemistry at McGill University in 2012 and went on to complete his MSc degree in chemistry, specializing in centrifugal microfluidics applied to analytical chemistry in 2014. Currently, he is a PhD candidate in the Department of Chemistry in Professor Wiseman's laboratory, using nonlinear microscopy to investigate biological tissues.

Angelica A. Gopal received her MSci (Hons) degree in chemistry with an international study year from the University of Nottingham in 2011, specializing in physical chemistry. She is completing her PhD in the Department of Chemistry in Professor Wiseman's laboratory, using image analysis techniques applied to biological systems.

Marie-Pier Girouard received her BSc degree in biochemistry from the Université de Sherbrooke in 2010. Currently, she is pursuing her PhD studies in the integrated program of neuroscience at McGill University in the laboratory of Professor Alyson Fournier.

Alyson E. Fournier is a full professor in neurology and neurosurgery at McGill University. Her research lab is at the Montreal Neurological Institute and studies molecular and cellular responses to central nervous system injury to develop therapeutic strategies to promote repair.

Paul W. Wiseman received his BSc degree from St. Francis Xavier University in 1989 and his PhD from the University of Western Ontario in 1995. In 2001, he started as an assistant professor jointly appointed in the Departments of Chemistry and Physics at McGill University, was promoted to associate professor in both departments in 2007, and to full professor in 2013. His research focuses on biophysics measurements of protein interactions and transport in living cells and neurons.